RSC Advances

PAPER

Cite this: *RSC Adv.*, 2021, **11**, 15581

Photoluminescence and scintillation characteristics of Bi-loaded PVK-based plastic scintillators for the high counting-rate measurement of high-energy X-rays†

Atsushi Sato, *[a] Arisa Magi,[a] Masanori Koshimizu,[a] Yutaka Fujimoto,[a] Shunji Kishimoto[b] and Keisuke Asai[a]

We synthesized Bi-loaded poly(9-vinylcarbazole) (PVK)-based plastic scintillators for high-energy X-ray detection. PVK, triphenylbismuth ($BiPh_3$), and 1,4-bis(2-methylstyryl)benzene (bis-MSB) served as the host polymer, heavy metal compound, and organic phosphor, respectively. The emission peaks at approximately 440 nm in the photoluminescence emission and X-ray-excited radioluminescence spectra of the synthesized scintillators are attributed to bis-MSB. The scintillation decay time constants of the 1st exponential components are 1.6 ns. The presence of $BiPh_3$ in the synthesized scintillators successfully enhanced their efficiency in the detection of 67.41 keV X-rays. The detection efficiency per 1 mm thickness achieved by a PVK-based plastic scintillator loaded with 10 wt% Bi was 2.5-times higher than that achieved by a commercial polyvinyltoluene (PVT)-based plastic scintillator loaded with 5 wt% Pb, EJ-256. The light yield of the PVK-based plastic scintillator loaded with 10 wt% Bi was 5600 photons per MeV, which was higher than that of EJ-256. We successfully enhanced the high-energy X-ray detection efficiency of PVK-based plastic scintillators, through the addition of $BiPh_3$, while maintaining a short decay time of nanoseconds.

Received 10th March 2021
Accepted 16th April 2021

DOI: 10.1039/d1ra01878g

rsc.li/rsc-advances

Introduction

The rapid detection of high-energy photons required in various X-ray applications at synchrotron radiation facilities is driving the demand for scintillators with fast scintillation decay, high detection efficiency, and high light yield.[1] Such scintillators are also required in the development of next-generation medical imaging diagnostic technology, such as photon-counting computed tomography[2] and time-of-flight positron emission tomography.[3] However, no scintillators satisfy all these requirements. When the low-energy X-rays of less than 20 keV are used at high counting-rate in synchrotron X-ray experiments, silicon avalanche photodiode detectors (Si-APDs) have been used.[4,5] Although it is possible for Si-APDs to measure the low-energy X-rays at high-counting rate, the detection efficiency for the high-energy X-rays of higher than 20 keV is low due to the active layer thickness of 10–150 μm and the small atomic number of the constitute element, Si.[6] The detection efficiency can be increased with an increase in the thickness of the active layer of the Si-APD, however, the time resolution would be worsen. As a result, scintillators with fast scintillation decay and high detection efficiency for high-energy X-rays (higher than 20 keV) are required.

Examples of reported inorganic scintillators that achieve rapid detection and demonstrate high detection efficiency are based on Ce- or Pr-doped single crystals[7–10] or materials that exhibit Auger-free luminescence.[11–13] Although these scintillators demonstrate fast scintillation decay, their performance in terms of the fast detection of high-energy photons is limited. The Ce or Pr luminescence centers employed in Ce- and Pr-doped single crystal scintillators, respectively, produce scintillation decay times of several tens of nanoseconds. On the other hand, the light yield of scintillators employing materials that exhibit Auger-free luminescence of 500–1400 photons per MeV (ref. 11–13) is lower than those of other inorganic scintillators, and results in the low energy resolution of high-energy photons. In addition, a long scintillation decay time of 630 ns observed for inorganic scintillators based on BaF_2 is due to the large proportion of excitons that become self-trapped in BaF_2.[11] Unlike those of inorganic scintillators, the scintillation decay times of organic scintillators are generally short (a mere several nanoseconds). This study focuses on plastic scintillators, which are a type of organic scintillators. Plastic scintillators are based on organic phosphors that feature short scintillation decay

[a]*Department of Applied Chemistry, Graduate School of Engineering, Tohoku University, 6-6-07 Aoba, Aramaki, Aoba-ku, Sendai 980-8579, Japan. E-mail: atsushi.sato.r2@dc.tohoku.ac.jp*

[b]*High-Energy Accelerator Research Organization, 1-1 Oho, Tsukuba 305-0801, Japan*

† Electronic supplementary information (ESI) available. See DOI: 10.1039/d1ra01878g

times of 0.7–3.0 ns.[14,15] However, the efficiency of plastic scintillators in detecting high-energy photons is low because of the small atomic numbers of their constituent elements, which are C, H, N, and O. Several studies have explored the addition of heavy metals to enhance the high-energy photon detection efficiency of plastic scintillators. Heavy metals, such as Zr,[16,17] Sn,[18,19] Hf,[20–22] Pb,[19,23,24] and Bi,[25–30] have been added to host polymers, such as polystyrene (PS), polyvinyltoluene (PVT), and poly(9-vinylcarbazole) (PVK).[31,32] Presently, several suppliers offer commercial plastic scintillators loaded with 1–7 wt% Pb: Eljen Technology, OKEN, Saint-Gobain, or IHEP (EJ-256, NE142, BC-452, SC-223, SC-322), which are available for high-energy photon detection. Commercial plastic scintillators loaded with 1.7–5 wt% Sn are also available (NE140, SC-221, SC-222, SC-321). The detection efficiency of these Pb-loaded plastic scintillators is limited by the solubility of Pb in the polymer solvent. Also loading of Pb into PS or PVT at high concentration results in a dramatic reduction of light yield, owing to which the detection efficiency will be worsen. As a result, the concentration of Pb added to PS or PVT is limited. In previous studies, we successfully enhanced the detection efficiency of PS-based plastic scintillators through the addition of surface-modified HfO_2 or Bi_2O_3 nanoparticles prepared *via* subcritical hydrothermal synthesis.[21,28] In particular, the detection efficiency per unit thickness and the light yield of a PS-based plastic scintillator loaded with surface-modified Bi_2O_3 nanoparticles were 1.6 and 1.1 times higher, respectively, than those of EJ-256 (Eljen Technology),[33] which is loaded with 5 wt% Pb. Whereas, the detection efficiency per unit thickness and the light yield of a PS-based plastic scintillator featuring HfO_2-loaded organo-silica nanoparticles synthesized *via* sol–gel method were 2 and 1.2 times higher, respectively, than those of EJ-256.[22]

Bi has a higher atomic number than Pb or Hf, and for the development of plastic scintillators, has been incorporated into host polymers in various forms, *e.g.* nanoparticles,[28] or as constituents or inorganic compounds[27] and organometallic species.[29,30] In previous studies, triphenylbismuth ($BiPh_3$) was incorporated into PS-based plastic scintillators to enhance their high-energy photon detection efficiency.[29,30] Although the detection efficiency was successfully enhanced, an undesirable reduction in light yield was observed, which was directly correlated with the concentration of Bi. In another study, PVK was used to host $BiPh_3$.[34] Like PS and PVT, PVK is a vinyl polymer that has side chains featuring π-electron systems, and demonstrates excellent photoconductivity as an organic electroluminescence material.[35] A $BiPh_3$-loaded PVK-based plastic scintillator reportedly delivers high light yield suitable for gamma-ray spectroscopy.[34] In the PVK-based plastic scintillator, bis(3,5-difluoro-2-(2-pyridyl)phenyl-(2-carboxypyridyl)iridium(III)) (FIrpic) was used as a phosphor. A PVK-based plastic scintillator without Bi produced a light yield of approximately 24 000 photons per MeV, which mostly originated from the triplet excited states of FIrpic. The photoluminescence (PL) decay time obtained, using a flashlamp-pumped 266 nm Nd:YAG laser, was approximately 1200 ns, resulting from the phosphorescence of FIrpic. It was suggested that exciton transfer from $BiPh_3$, with a highest occupied molecular orbital (HOMO)–lowest unoccupied molecular orbital (LUMO) gap of 4.1 eV, to PVK, with a HOMO–LUMO gap of 3.5 eV, occurs because the HOMO–LUMO gap of $BiPh_3$ is wider than those of polymer matrices employed in previous studies. As a result, the light yield under 662 keV gamma-radiation from ^{137}Cs increased by 1.07% after loading the FIrpic-containing, PVK-based plastic scintillator with 40% $BiPh_3$. Furthermore, a PVK-based plastic scintillator loaded with an Ir(III)-complex phosphor, tris[2-(*p*-tolyl)pyridine]iridium(III) ($Ir(mppy)_3$), delivered a light yield of more than 30 000 photons per MeV.[36] However, its PL decay time was approximately 850 ns. Unlike conventional plastic scintillators, these FIrpic- or $Ir(mppy)_3$-loaded plastic scintillators do not have short PL lifetimes of several nanoseconds, because the light emission of these plastic scintillators derive from the phosphorescence of the Ir(III)-complex phosphors. Additionally, PVK-based plastic scintillator doped with organic phosphor, 9,10-diphenylanthracene (DPA), showed a light yield of more than 10 000 photons per MeV after loading of 40% $BiPh_3$ and a PL decay time of 14 ns.[34] Although the PL decay time was very shorter than that of PVK-based plastic scintillators doped with Ir(III)-complex phosphor, a short decay time of several nanoseconds was not obtained. There is currently a trade-off between fast scintillation decay, high detection efficiency, and high light yield; accordingly, no plastic scintillator demonstrates all three of these characteristics.

This study investigates PVK-based plastic scintillators loaded with $BiPh_3$. We used 1,4-bis(2-methylstynyl)benzene (bis-MSB), which has often been used in liquid scintillators as the organic phosphor.[37,38] We report the fabrication and high-energy X-ray detection characteristics of Bi-loaded PVK-based plastic scintillators that achieve fast detection and superior high-energy X-ray detection efficiency.

Experimental

PVK (average $M_w \approx 1\,100\,000$, Sigma-Aldrich), $BiPh_3$ (Tokyo Chemical Industry, 98+%), bis-MSB (Tokyo Chemical Industry, 99+%), and tetrahydrofuran (THF, Fujifilm Wako Pure Chemical, 99.5%) were used without further purification. In the fabrication of plastic scintillators specimens, PVK, $BiPh_3$, and bis-MSB served as the host polymer, heavy metal compound, and organic phosphor, respectively. The total weight of each prepared sample was 0.3 g. PVK was dissolved in 5 g of THF in a 20 mL screw vial before successively adding and dissolving (with stirring) $BiPh_3$ and bis-MSB. After the compounds had completely dissolved, the screw vial was sealed by aluminum foil with a hole of approximately 1 mm in diameter. The samples with a thickness of 0.2–0.4 mm were obtained after evaporating the solvent by heating the solution at 50 °C for 3 days. The molar percentage of bis-MSB relative to the 9-vinylcarbazole monomer units in each sample was 1 mol%. The samples were loaded with $BiPh_3$ to achieve weight percentages of Bi, relative to the total sample weight ranging from 0 to 15 wt%. In addition, a ~1 mm-thick Bi-loaded plastic scintillator was synthesized to determine the effect of thickness on performance. The total weight of this sample was 1.5 g and it

was synthesized in a 20 mL screw vial. The sample was loaded with $BiPh_3$ to realize a Bi content of 10 wt% and the molar percentage of bis-MSB relative to the 9-vinylcarbazole monomer units was 1.0 mol%.

Excitation–emission spectra at room temperature were measured using a fluorescence spectrophotometer (Hitachi, F-7000) equipped with a Xe lamp, which is the excitation source. X-ray-excited radioluminescence (XRL) spectra were recorded at room temperature using a multichannel spectrometer (Ocean Insight, QEPro) and an X-ray source, an X-ray generator (Rigaku, SA-HFM3) with a Cu target operating at 40 kV and 40 mA. PL temporal profiles were recorded on a fluorescence lifetime spectrofluorometer (Horiba, DeltaFlex 3000U-TMK2); the samples were excited using a pulsed light emitting diode (LED) and the excitation and emission wavelengths were 326 and 440 nm, respectively. An optical cut-off filter was used to limit interference by scattered excitation radiation. The approximation level was presented using chi-square value (χ^2). To record the scintillation temporal profiles, a delayed coincidence method was employed.[39] We used two 511 keV gamma rays oriented in opposite directions and generated by the annihilation of positrons emitted during the β^+ decay of ^{22}Na. Furthermore, ^{22}Na decays to an excited state of ^{22}Ne *via* β+ decay, and ^{22}Ne subsequently decays to its ground state by emitting a 1.275 MeV gamma-ray photon. The 1.275 MeV and two 511 keV gamma-rays are generated within the positron lifetime in the gamma-ray source of less than several hundreds of ps, which is shorter than the time resolution of the measurement system. Hence, the 1.275 MeV gamma-rays are also used for timing and excitation of the samples. A scintillation detector and the relevant sample were each irradiated with a 511 keV gamma ray. The scintillation detector consisting of a photomultiplier tube (PMT; Hamamatsu Photonics, H3378-51) and a Pilot-U plastic scintillator was used to determine the timing of gamma-ray generation. The relevant sample and scintillation detector were placed on opposite sides of the ^{22}Na source. A PMT (Hamamatsu Photonics, R7400P) was used to detect the scintillation photons emitted from the samples during time-correlated single-photon counting. The PMT was approximately 5 cm away from the relevant sample, because the average number of detected photons per gamma-ray photon should be less than 1. The detection signals from the scintillation detector and the PMT were converted into timing signals by a constant fraction discriminator (CFD; ORTEC, 935). The timing signals from the PMT were fed to a nanosecond delay (ORTEC, 425A). A time-to-amplitude converter (TAC; ORTEC, 566) converted the start signals from the scintillation detector and the stop signals from the PMT into output signals that were relayed to a multichannel analyzer (MCA; Amptek, MCA 8000D) to produce scintillation temporal profiles. The approximation level was presented using χ^2 like PL temporal profiles. The high-energy X-ray detection characteristics of the samples were evaluated using a synchrotron X-ray beam at beamline BL-14A of Photon Factory, KEK, Japan, operating in hybrid mode. The focal spot of the X-ray beam had dimensions of approximately 1 mm × 1 mm. The measurement procedure is described in a previous article.[40] Each sample was attached to the glass window of a PMT (Hamamatsu Photonics, R7400P) with optical grease and covered with Teflon tape that served as a reflector. The pulse-height spectra were recorded using X-radiation with an energy of 67.41 keV, which is equivalent to the energy of the first excited level of ^{61}Ni,[41] because we expect to apply the scintillators in the measurement of the nuclear resonant scattering of ^{61}Ni.[42] The detection signals were amplified with a charge-sensitive preamplifier (Canberra, 2005) and a main amplifier (ORTEC, 572A, shaping time: 0.5 μs), and then fed to an MCA (Amptek, MCA 8000D). The detection efficiency achieved by each scintillator sample was estimated by comparing the obtained count rate with that of a scintillation detector equipped with 5 mm-thick NaI:Tl, whose efficiency in detecting 67.41 keV X-rays was assumed to be 100%. The 67.41 keV X-rays was assumed to be fully in NaI:Tl with a thickness of 5 mm according to the estimation with the NIST table. In addition, the absorbed X-ray photons are estimated to be detected with a probability of almost 100%, because the detection signals of I escape peaks were also taken into account. To estimate the light yield of the samples, the recorded photopeak channels were compared with that of 2 mm-thick EJ-256, which has a light yield of 5200 photons per MeV.[33] To acquire time profiles of the detection signals, the detection signals from the PMT were amplified with a fast preamplifier (ORTEC, VT120A), and the timing of the signals was determined with a CFD (ORTEC, 935). The acquisition threshold potential for the start signals was set to 20 mV, at which input signals including one-photon signals were recorded. The stop signals were synchronized with the timing of electron acceleration in the accelerator. The time differences between the start and stop signals were converted into voltages (output signals) with a TAC (ORTEC, 566) that were relayed to an MCA to produce time profiles. The time resolution is defined as the full width at half maximum (FWHM) of the peak of the time profile. The high-energy X-ray detection characteristics of the Bi-loaded PVK-based plastic scintillators were compared with those of EJ-256.

Results and discussion

Fig. 1(a) shows photographs of plastic scintillator samples loaded with different weights of Bi under visible light; all the samples are transparent. Fig. 1(b) displays photographs of the samples under 302 nm ultraviolet (UV) radiation; all the

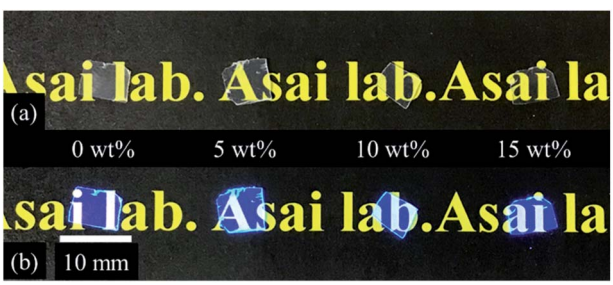

Fig. 1 Photographs of synthesized plastic scintillators under (a) visible light and (b) 302 nm UV radiation.

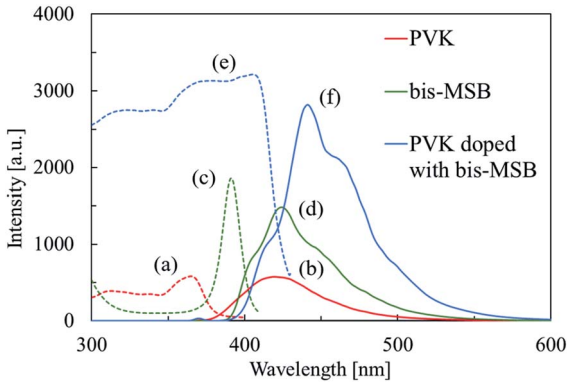

Fig. 2 PL excitation spectra (dashed lines) and emission spectra (solid lines) of PVK (a: $\lambda_{em} = 419$ nm, b: $\lambda_{ex} = 365$ nm), bis-MSB in ethanol (c: $\lambda_{em} = 420$ nm, d: $\lambda_{ex} = 390$ nm) and PVK containing bis-MSB (e: $\lambda_{em} = 442$ nm, f: $\lambda_{ex} = 365$ nm).

samples emit blue light. The synthesized samples have thickness in the range 0.20–0.40 mm.

Fig. 2 shows the PL excitation and emission spectra of PVK, bis-MSB in ethanol, and PVK containing bis-MSB. The spectrum of PVK containing bis-MSB shows the excitation bands of both PVK and bis-MSB in ethanol. The PL peak in the spectrum of PVK containing bis-MSB appears at a wavelength approximately 20 nm greater than that in the spectrum of bis-MSB in ethanol. The emission spectrum of PVK containing bis-MSB (Fig. 2) is consistent with previously reported emission spectra of PVK films doped with bis-MSB.[43] The shift of the PL peak associated with bis-MSB to longer wavelengths is caused by its host. Fig. 3 shows the PL excitation and emission spectra of the Bi-free and Bi-loaded PVK-based plastic scintillators. Each excitation spectrum shows a broad band between 350 and 410 nm, with a PL peak and two shoulders at approximately 440, 410 and 460 nm, respectively.

Fig. 4 shows the XRL spectra of the Bi-free and Bi-loaded PVK-based plastic scintillators. The XRL spectra are similar to the PL emission spectra and the emission is attributed to bis-MSB. Additionally, the wavelength of the emission peak in the spectrum of the thick sample is approximately 20 nm greater

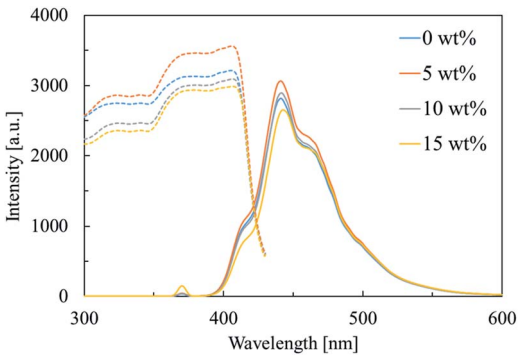

Fig. 3 PL excitation spectra (dashed) at $\lambda_{em} = 442$ nm and emission spectra (solid) at $\lambda_{ex} = 365$ nm of Bi-free and Bi-loaded PVK-based plastic scintillators.

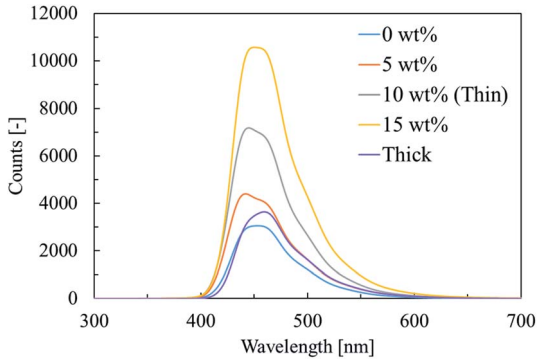

Fig. 4 XRL spectra of Bi-free and Bi-loaded PVK-based plastic scintillators.

than that of the emission peak in the spectrum of the thin sample. In Fig. 3, the wavelengths of the peaks of the PL emission and excitation spectra of the Bi-free and Bi-loaded PVK-based plastic scintillators are approximately 440 and 410 nm, respectively, *i.e.* a difference of approximately 30 nm. Scintillation photons emitted by the samples pass through the samples to the multichannel spectrometer during the measurement of the XRL spectra and some of these scintillation photons are likely absorbed by the samples. The incidence of self-absorption tends to increase with increasing sample thickness. In the case of the thick sample, the emission peak in its XRL spectrum appears at a longer wavelength than that in the XRL spectrum of the thin sample (Fig. 4), because the scintillation photons of shorter wavelengths are preferentially self-absorbed.

Fig. 5 shows the PL temporal profile of PVK. The excitation and emission wavelengths were 326 and 420 nm, respectively, and the duration of measurement was 400 ns. The temporal profile of PVK was approximated using two exponential functions. Table 1 lists the time constants of the exponential components of the PL decay of PVK, *i.e.*, 11 and 32 ns. It was previously reported that the time constants of the 1st and 2nd exponential components of the PL decay of a PVK film were 16.6 and 30.5 ns, respectively,[44] which were attributed to PVK monomer and excimer emission, respectively. The obtained time constants of the 1st and 2nd exponential components of

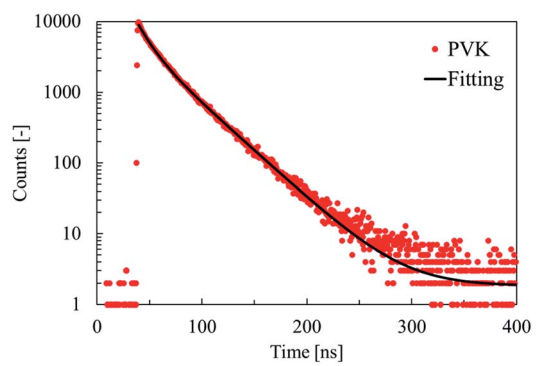

Fig. 5 PL temporal profile of PVK ($\lambda_{ex} = 326$ nm, $\lambda_{em} = 420$ nm).

Table 1 Time constants of the exponential components of the PL decay of PVK

Decay time constant		χ^2
τ_1 [ns]	11 (50%)	1.3
τ_2 [ns]	32 (50%)	

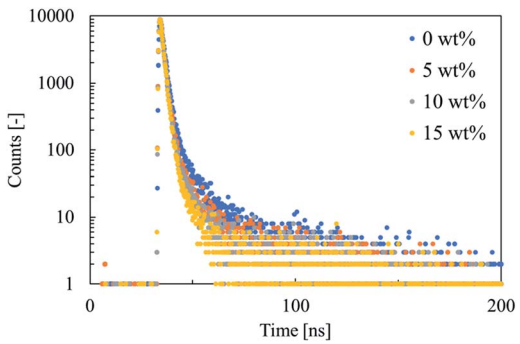

Fig. 6 PL temporal profiles of Bi-free and Bi-loaded PVK-based plastic scintillators (λ_{ex} = 326 nm, λ_{em} = 440 nm).

the PL decay of PVK are consistent with those previously reported.

Fig. 6 shows the PL temporal profiles of the Bi-free and Bi-loaded PVK-based plastic scintillators. The excitation and emission wavelengths were 326 and 440 nm, respectively, and the duration of measurement was 200 ns. The obtained temporal profiles were deconvoluted with the instrumental response function, and the sum of two exponential functions was used to approximate the temporal profiles. Table 2 lists the time constants of the exponential components of PL decay of Bi-free and Bi-loaded PVK-based plastic scintillators. The time constants of the 1st exponential components of PL decay are 1.4–1.8 ns, consistent with the time constant of PL decay of bis-MSB in cyclohexane (1.56 ± 0.05 ns).[45] The irradiation of PVK-based plastic scintillators, using a pulsed LED that produces light with a wavelength of 326 nm, mainly excites the PVK and part of this energy subsequently transfers from PVK to bis-MSB. Therefore, the PL decay time constants of the 1st exponential components are attributed to the PL decay of bis-MSB based on its time constant and the PL emission spectra in Fig. 2. Moreover, the time constants of the 1st exponential components of the PL decay of the PVK-based plastic scintillators decrease with increasing $BiPh_3$ content. $BiPh_3$ is reportedly a PL quencher.[46] Part of the energy transferred from PVK to bis-MSB, in turn, transfers to $BiPh_3$ and is quenched. The PL decay time constants of the 2nd exponential components are 7.0–12 ns, which approach the time constant of the 1st exponential component of the PL decay of PVK (Table 1). According to the PL temporal profile of PVK at an emission wavelength of 440 nm, the time constant of the 1st exponential component of its PL decay is 19 ns; this is higher than the time constants of the 2nd exponential components of the PL decay of the Bi-free and Bi-loaded PVK-based plastic scintillators. However, the emission derived from PVK is not clearly observed in the PL spectra in Fig. 3, likely obscured by the emission of bis-MSB. In the cases of the Bi-free and Bi-loaded PVK-based plastic scintillators, the time constants of the 2nd exponential components of their PL decay are attributed to the PL decay of PVK. The PL decay time constants of the 2nd exponential components decrease with increasing $BiPh_3$ content owing to the energy transfer from PVK to $BiPh_3$.

Table 2 Time constants of the exponential components of the PL decay of Bi-free and Bi-loaded PVK-based plastic scintillators

	Decay time constant		
Sample	τ_1 [ns]	τ_2 [ns]	χ^2
Bi 0 wt%	1.8 (99%)	12 (1%)	1.2
Bi 5 wt%	1.5 (99%)	9.1 (1%)	1.0
Bi 10 wt%	1.5 (99%)	8.7 (1%)	0.85
Bi 15 wt%	1.4 (99%)	7.0 (1%)	0.77

Fig. 7 shows the scintillation temporal profiles of Bi-free and Bi-loaded PVK-based plastic scintillators under 511 keV gamma radiation. The sum of two exponential functions was used to approximate the temporal profiles. Table 3 lists the time constants of the exponential components of the scintillation decay of Bi-free and Bi-loaded PVK-based plastic scintillators. The time constants of the 1st exponential components of scintillation decay are 1.6 ns, which are consistent with the PL decay time constants of the 1st exponential components (1.4–1.8 ns, in Table 2). The time constants of the 1st exponential components of scintillation decay derive from the scintillation decay of bis-MSB.[45] The scintillation decay time constants of the 2nd exponential components are 11–12 ns, which approach the PL

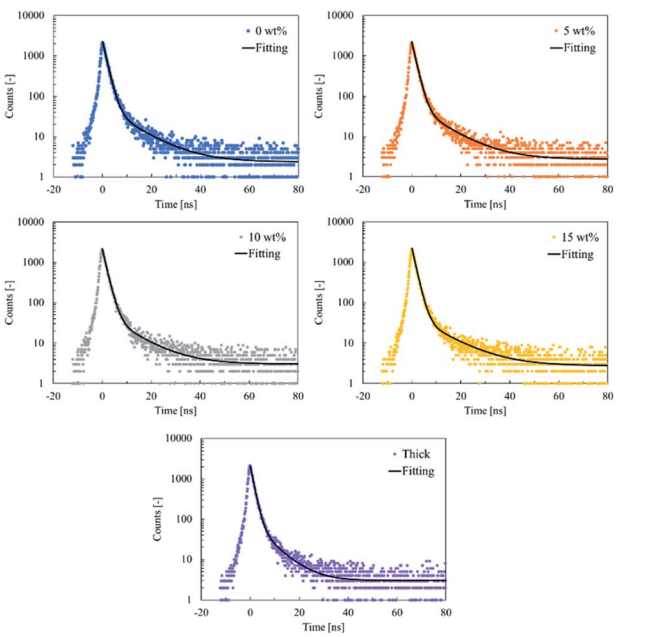

Fig. 7 Scintillation temporal profiles of Bi-free and Bi-loaded PVK-based plastic scintillators under 511 keV gamma radiation.

Table 3 Time constants of the scintillation decay of Bi-free and Bi-loaded PVK-based plastic scintillators

	Decay time constant		
Sample	τ_1 [ns]	τ_2 [ns]	χ^2
Bi 0 wt%	1.6 (98%)	11 (2%)	1.7
Bi 5 wt%	1.6 (97%)	11 (3%)	0.89
Bi 10 wt%	1.6 (98%)	11 (2%)	1.4
Bi 15 wt%	1.6 (98%)	12 (2%)	1.3
Thick	1.4 (96%)	7.0 (4%)	0.77

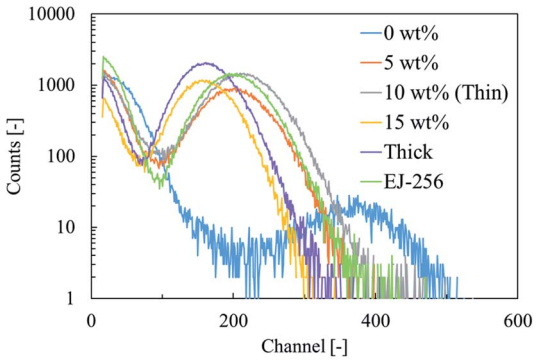

Fig. 8 Pulse-height spectra of scintillation detectors equipped with Bi-free and Bi-loaded PVK-based plastic scintillators and EJ-256 under 67.41 keV X-radiation.

decay time constants of the 2nd exponential components (Table 2). However, the emission deriving from PVK is not clearly observed in the XRL spectra in Fig. 4, likely obscured by the emission of bis-MSB. The time constants of the 2nd exponential components of the scintillation decay of Bi-free and Bi-loaded PVK-based plastic scintillators are attributed to the scintillation decay of PVK. There is minimal variation between the time constants of the scintillation decay exponential components of the Bi-free and Bi-loaded PVK-based plastic scintillators, unlike between the time constants of the corresponding PL decay exponential components. On the other hand, the time constants of the 1st and 2nd exponential components of the scintillation decay of the thick sample are lower than those of the corresponding exponential components of the scintillation decay of the thin sample. Additionally, the slow rise time of the temporal profiles is attributed to the energy transfer from PVK to bis-MSB.

Fig. 8 shows the pulse-height spectra of scintillation detectors exposed to 67.41 keV X-rays. The detection efficiency of the Bi-free and Bi-loaded PVK-based plastic scintillators was estimated by comparing their count rates with that of a scintillation detector equipped with 5 mm-thick NaI:Tl, whose efficiency in detecting 67.41 keV X-rays was assumed to be 100%. Table 4 lists the detection efficiencies per 1 mm thickness of scintillation detectors equipped with Bi-free and Bi-loaded PVK-based plastic scintillators, and EJ-256. The detection efficiencies of the PVK-based plastic scintillators loaded with 5, 10, and 15 wt% Bi (3.2, 6.5, and 8.3%, respectively) are 1.2, 2.5, and 3.2 times higher, respectively, than that of EJ-256. The detection efficiency of the PVK-based plastic scintillators increases with increasing Bi content, which indicates that the probability of scintillator–X-ray interaction is enhanced by the presence of $BiPh_3$. The pulse-height spectra of Bi-loaded PVK-based plastic scintillators show distinct photo-peaks that shift to lower channels with increasing Bi content. The presence of $BiPh_3$, as a quencher, in a PVK-based plastic scintillators reduces its light yield. To estimate the light yield of each scintillator, the photo-peak channels in the pulse-height spectra of the samples were compared with that of the pulse-height spectrum of EJ-256; Table 4 lists the results. The light yields of PVK-based plastic scintillators loaded with 0, 5, and 10 wt% Bi are 9900, 5300, and 5600 photons per MeV, respectively, which exceed that of EJ-256. Furthermore, Table 4 lists the energy resolutions of the Bi-free and Bi-loaded PVK-based plastic scintillators and EJ-256. The Bi-loaded PVK-based plastic scintillators show an energy resolution of 46–51%, which is comparable to that EJ-256 of 46%. Furthermore, the detection efficiency of the thick sample is 5.2%, which is slightly higher than that of the 2 mm-thick EJ-256 and 3.3 times higher than that of the thin sample. The thick sample is 3.8 times thicker than the thin sample, indicating that the detection efficiency of the scintillator is almost proportional to its thickness. The light yield of the thick sample is 4300 photons per MeV; this value is not corrected to account for the difference in the XRL peak wavelengths of the sample because there was little difference between the quantum efficiency of the PMT (HAMAMATSU, R7400P)[47] at these wavelengths. The lower light yield of the thick sample, which is 0.77 times that of the thin sample, is owed to the higher incidence of self-absorption in the thick sample.

Table 4 Detection efficiencies per 1 mm thickness of scintillation detectors equipped with Bi-free and Bi-loaded PVK-based plastic scintillators, and EJ-256; and corresponding light yields and energy resolutions under 67.41 keV X-radiation

Samples	Thickness [mm]	Detection efficiency [%]	Detection efficiency [%] (1 mm of conversion)	Light yield [photons per MeV]	Energy resolution [%]
Bi 0 wt%	0.40	0.51	1.3	9900	35
Bi 5 wt%	0.34	1.1	3.2	5300	49
Bi 10 wt%	0.24	1.6	6.5	5600	46
Bi 15 wt%	0.36	3.0	8.3	4200	51
Thick	0.90	5.2	5.8	4300	50
EJ-256	2.00	5.1	2.6	5200	46

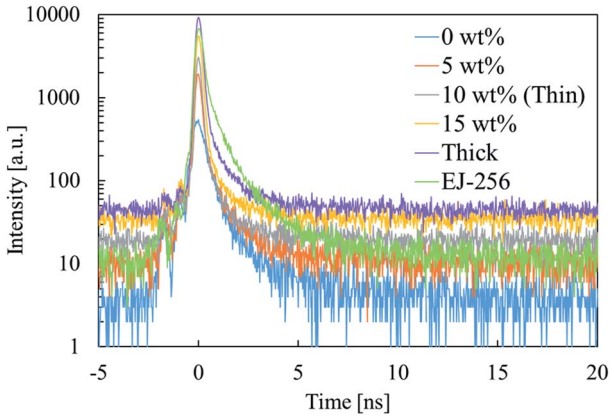

Fig. 9 Time profiles of detection signals of scintillation detectors equipped with Bi-free and Bi-loaded PVK-based plastic scintillators, and EJ-256 under 67.41 keV X-radiation.

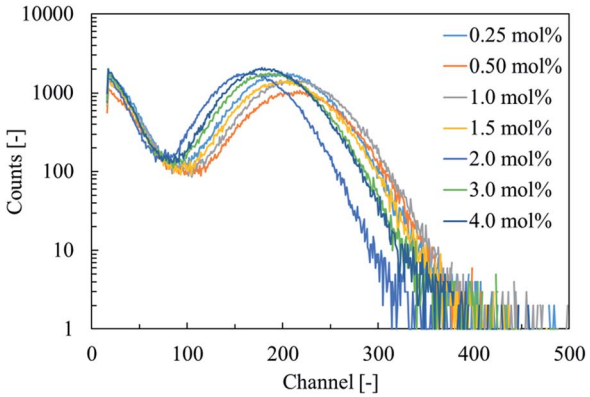

Fig. 10 Pulse-height spectra of scintillation detectors equipped with Bi-loaded PVK-based plastic scintillators with different bis-MSB contents under 67.41 keV X-radiation.

Fig. 9 shows the time profiles of the detection signals of scintillation detectors equipped with Bi-free and Bi-loaded PVK-based plastic scintillators and EJ-256 under 67.41 keV X-radiation. All the PVK-based plastic scintillators achieved, a time resolution of less than 1 ns, and long tails are not observed in the time profiles of their detection signals in Fig. 9. The baselines of the time profiles shift to higher intensities, possibly owing to afterglow artifacts caused by X-ray irradiation. Table 5 lists the time resolution of Bi-free and Bi-loaded PVK-based plastic scintillators, and EJ-256 under 67.41 keV X-radiation. The time resolution is estimated by the FWHM of the peak of each time profile. The time resolution of the PVK-based plastic scintillator is reduced by the presence of $BiPh_3$. The time resolution of the Bi-loaded PVK-based plastic scintillators is 0.28–0.31 ns, which is almost independent of their Bi content. Accordingly, the Bi-loaded PVK-based plastic scintillators achieved better time resolution than EJ-256. Additionally, the time resolution curves of the thick and thin samples do not differ. The time resolution achieved by the thick sample is 0.33 ns, which is lower than that achieved by the thin sample.

The organic phosphor content of PVK-based plastic scintillators loaded with 10 wt% Bi was optimized. Bi-loaded PVK-based plastic scintillators were prepared in which the molar percentage of bis-MSB relative to the 9-vinylcarbazole monomer units ranged from 0.25 to 4.0 mol%. Fig. 10 shows the pulse-height spectra of scintillation detectors equipped with Bi-loaded PVK-based plastic scintillators with different bis-MSB contents under 67.41 keV X-radiation. The channels of the photopeaks in the spectra of the samples containing 0.25–1.5 mol% bis-MSB were almost the same. The light yield of the Bi-loaded PVK-based plastic scintillators shows limited dependence on the bis-MSB content. The scintillator containing 1.0 mol% bis-MSB achieves the highest light yield.

Table 5 Time resolution of Bi-free and Bi-loaded PVK-based plastic scintillators, and EJ-256 under 67.41 keV X-radiation

Samples	Time resolution [ns]
Bi 0 wt%	0.62
Bi 5 wt%	0.31
Bi 10 wt%	0.28
Bi 15 wt%	0.31
Thick	0.33
EJ-256	0.43

Conclusions

The PL and scintillation characteristics of Bi-loaded PVK-based plastic scintillators were evaluated during high counting-rate measurements of high-energy X-rays. The PL emission and XRL spectra of Bi-loaded PVK-based plastic scintillators reflected peaks at approximately 440 nm derived from bis-MSB. The Bi-loaded PVK-based plastic scintillators exhibited a short decay time of 1.6 ns. The detection efficiency per 1 mm thickness of PVK-based plastic scintillator loaded with 10 wt% Bi was 6.5%, which was 2.5 times higher than that of EJ-256. PVK containing bis-MSB achieved a light yield of 9900 photons per MeV, which decreased with increasing Bi content. The light yield of the PVK-based plastic scintillator loaded with 10 wt% Bi was 5600 photons per MeV, which was higher than that of EJ-256. All the PVK-based plastic scintillators achieved nanosecond scintillation decay time. Moreover, the time resolution achieved by the Bi-loaded PVK-based plastic scintillators was superior to that of EJ-256. Therefore, we successfully enhanced the detection efficiency of PVK-based plastic scintillators, while maintaining short decay time of nanoseconds, by incorporating $BiPh_3$. The incidence of self-absorption increased with increasing thickness of the Bi-loaded PVK-based plastic scintillators, resulting in a slight reduction in the light yield. The detection efficiency of a 0.90 mm-thick sample exceeded that of 2 mm-thick EJ-256. These results indicate that Bi-loaded PVK-based plastic scintillators are applicable for high counting-rate measurement of high-energy X-rays. For the application to the measurement of the nuclear resonant scattering of ^{61}Ni, a significant enhancement in the light yield of plastic scintillators is necessary.

Conflicts of interest

There are no conflicts to declare.

Acknowledgements

This research was supported by a Grant-in-Aid for Scientific Research (A) (Grant No. 18H03890, 2018–2021). Part of this research is based on the Cooperative Research Project of the Research Center for Biomedical Engineering, Ministry of Education, Culture, Sports, Science and Technology.

References

1 R. Haruki, K. Shibuya, F. Nishikido, M. Koshimizu, Y. Yoda and S. Kishimoto, *J. Phys.: Conf. Ser.*, 2010, **217**, 012007.
2 M. J. Willemink, M. Persson, A. Pourmorteza, N. J. Pelc and D. Fleiscbmann, *Radiology*, 2018, **289**, 293–312.
3 S. Gundacker, R. M. Turtos, N. Kratochwil, R. H. Pots, M. Paganoni, P. Lecoq and E. Auffray, *Phys. Med. Biol.*, 2020, **65**, 025001.
4 S. Kishimoto, *Nucl. Instrum. Methods Phys. Res., Sect. A*, 1991, **309**(3), 603–605.
5 S. Kishimoto, *Rev. Sci. Instrum.*, 1992, **63**, 824–827.
6 A. Q. R. Baron, S. Kishimoto, J. Morse and J. M. Rigal, *J. Synchrotron Radiat.*, 2006, **13**, 131–142.
7 M. Moszyriski, D. Wolski, T. Ludziejewski, M. Kapusta, A. Lempicki, C. Brecher, D. Wisniewski and A. J. Wojtowicz, *Nucl. Instrum. Methods Phys. Res., Sect. A*, 1997, **385**, 123–131.
8 M. Moszynski, M. Kapusta, D. Wolski, W. Klamra and B. Cederwall, *Nucl. Instrum. Methods Phys. Res., Sect. A*, 1998, **404**, 157–165.
9 Y. Yoshida, K. Shinozaki, T. Igashira, N. Kawano, G. Okada, N. Kawaguchi and T. Yanagida, *Solid State Sci.*, 2018, **78**, 1–6.
10 Y. Yoshida, G. Okada, N. Kawaguchi and T. Yanagida, *Optik*, 2019, **182**, 884–889.
11 P. Dorenbos, J. T. M. de Haas, R. Visser, C. W. E. van Eijk and R. W. Hollander, *IEEE Trans. Nucl. Sci.*, 1993, **40**(4), 424–430.
12 K. Takahashi, M. Koshimizu, Y. Fujimoto, T. Yanagida and K. Asai, *J. Ceram. Soc. Jpn.*, 2018, **126**, 755–760.
13 K. Takahashi, M. Arai, M. Koshimizu, Y. Fujimoto, T. Yanagida and K. Asai, *Jpn. J. Appl. Phys.*, 2020, **59**, 032003.
14 *Data sheet of EJ-212*, Eljen Technology.
15 *Data sheet of EJ-232Q*, Eljen Technology.
16 Y. Araya, M. Koshimizu, R. Haruki, F. Nishikido, S. Kishimoto and K. Asai, *Sens. Mater.*, 2015, **27**(3), 255–261.
17 A. Toda and S. Kishimoto, *IEEE Trans. Nucl. Sci.*, 2020, **67**(6), 983–987.
18 P. L. Feng, W. Mengesha, M. R. Anstey and J. G. Cordaro, *IEEE Trans. Nucl. Sci.*, 2016, **63**(1), 407–415.
19 G. I. Britvich, V. G. Vasil'chenko, V. G. Lapshin and A. S. Solov'ev, *Instrum. Exp. Tech.*, 2000, **43**, 36–39.
20 Y. Sun, M. Koshimizu, N. Yahaba, F. Nishikido, S. Kishimoto, R. Haruki and K. Asai, *Appl. Phys. Lett.*, 2014, **104**, 174104.
21 F. Hiyama, T. Noguchi, M. Koshimizu, S. Kishimoto, R. Haruki, F. Nishikido, T. Yanagida, Y. Fujimoto, T. Aida, S. Takami, T. Adschiri and K. Asai, *Jpn. J. Appl. Phys.*, 2018, **57**, 012601.
22 K. Kagami, M. Koshimizu, Y. Fujimoto, S. Kishimoto, R. Haruki, F. Nishikido and K. Asai, *J. Mater. Sci.: Mater. Electron.*, 2020, **31**, 896–902.
23 M. Hamel, G. Turk, A. Rousseau, S. Darbon, C. Reverdin and S. Normand, *Nucl. Instrum. Methods Phys. Res., Sect. A*, 2011, **660**, 57–63.
24 E. van Loef, G. Markosyan, U. Shirwadkar, M. McClish and K. S. Shah, *Nucl. Instrum. Methods Phys. Res., Sect. A*, 2015, **788**, 71–72.
25 G. H. V. Bertrand, J. Dumazert, F. Sguerra, R. Coulon, G. Corre and M. Hamel, *J. Mater. Chem. C*, 2015, **3**, 6006–6011.
26 Nerine J. Cherepy, R. D. Sanner, P. R. Beck, E. L. Swanberg, T. M. Tillotson, S. A. Payne and C. R. Hurlbut, *Nucl. Instrum. Methods Phys. Res., Sect. A*, 2015, **778**, 126–132.
27 K. Kagami, M. Koshimizu, Y. Fujimoto, S. Kishimoto, R. Haruki, F. Nishikido and K. Asai, *Radiat. Meas.*, 2020, **135**, 106361.
28 F. Hiyama, T. Noguchi, M. Koshimizu, S. Kishimoto, R. Haruki, F. Nishikido, T. Yanagida, Y. Fujimoto, T. Aida, S. Takami, T. Adschiri and K. Asai, *Jpn. J. Appl. Phys.*, 2018, **57**, 055203.
29 G. H. V. Bertrand, F. Sguerra, C. Dehe-Pittance, F. Carrel, R. Coulon, S. Normand, E. Barat, T. Dautremer, T. Montagu and M. Hamel, *J. Mater. Chem. C*, 2014, **2**, 7304–7312.
30 M. Koshimizu, G. H. V. Bertrand, M. Hamel, S. Kishimoto, R. Haruki, F. Nishikido, T. Yanagida, Y. Fujimoto and K. Asai, *Jpn. J. Appl. Phys.*, 2015, **54**, 102202.
31 M. Hamel and F. Carrel, *New Insights on Gamma Rays*, 2017, pp. 47–66.
32 T. J. Hajagos, C. Liu, N. J. Cherepy and Q. Pei, *Adv. Mater.*, 2018, **30**, 1706956.
33 *Data sheet of EJ-256*, Eljen Technology.
34 B. L. Rupert, N. J. Cherepy, B. W. Sturm, R. D. Sanner and S. A. Payne, *Europhys. Lett.*, 2012, **97**, 22002.
35 J. Kido, K. Hongawa, K. Okuyama and K. Nagai, *Appl. Phys. Lett.*, 1993, **63**, 2627–2629.
36 I. H. Campbell and B. K. Crone, *Appl. Phys. Lett.*, 2007, **90**, 012117.
37 Y. Ding, Z. Zhang, J. Liu, Z. Wang, P. Zhou and Y. Zhao, *Nucl. Instrum. Methods Phys. Res., Sect. A*, 2008, **584**, 238–243.
38 L. J. Bignell, D. Beznosko, M. V. Diwan, S. Hans, D. E. Jaffe, S. Kettell, R. Rosero, H. W. Themann, B. Viren, E. Worcester, M. Yeh and C. Zhang, *J. Instrum.*, 2015, **10**, P12009.
39 L. M. Bollinger and G. E. Thomas, *Rev. Sci. Instrum.*, 1961, **32**, 1044.
40 M. Koshimizu, K. Onodera, F. Nishikido, R. Haruki, K. Shibuya, S. Kishimoto and K. Asai, *J. Appl. Phys.*, 2012, **111**, 024906.
41 M. R. Bhat, *Nucl. Data Sheets*, 1999, **88**(3), 417–532.
42 S. Kishimoto, K. Shibuya, F. Nishikido, M. Koshimizu, R. Haruki and Y. Yoda, *Appl. Phys. Lett.*, 2008, **93**, 261901.

43 J. Ramsbrock, PhD thesis, Edinburgh Napier University, 2000.
44 S. Yan, M. Qin, C. Shen, L. Niu and Y. Zhang, *Synth. Met.*, 2020, **263**, 116368.
45 M. M de Souza, G. Rumbles, I. R. Gould, H. Amer, I. D. W. Samuel, S. C. Moratti and A. B. Holmesc, *Synth. Met.*, 2000, **111–112**, 539–543.
46 M. Hyman and J. J. Ryan, *IRE Trans. Nucl. Sci.*, 1958, **5**, 87–90.
47 *Datasheet of R7400U Series*, Hamamatsu.